PURPOSE-LED
PUBLISHING™

PAPER • OPEN ACCESS

Exact results on the dynamics of the stochastic Floquet-East model[*]

To cite this article: Cecilia De Fazio et al 2024 J. Phys. A: Math. Theor. **57** 505002

View the article online for updates and enhancements.

Exact results on the dynamics of the stochastic Floquet-East model*

Cecilia De Fazio[1,2,**] ⓘ **, Juan P Garrahan**[1,2] ⓘ
and Katja Klobas[1,2,3] ⓘ

[1] School of Physics and Astronomy, University of Nottingham, Nottingham NG7 2RD, United Kingdom
[2] Centre for the Mathematics and Theoretical Physics of Quantum Non-Equilibrium Systems, University of Nottingham, Nottingham NG7 2RD, United Kingdom
[3] School of Physics and Astronomy, University of Birmingham, Edgbaston, Birmingham B15 2TT, United Kingdom

E-mail: cecilia.de-fazio@mnf.uni-tuebingen.de

Abstract

We introduce a stochastic generalisation of the classical deterministic Floquet-East model, a discrete circuit with the same kinetic constraint as the East model of glasses. We prove exactly that, in the limit of long time and large size, this model has a large deviation phase transition between active and inactive dynamical phases. We also compute the finite time and size scaling of general space-time fluctuations, which for the case of inactive regions gives rise to dynamical hydrophobicity. We also discuss how, through the Trotter limit, these exact results also hold for the continuous-time East model, thus proving long-standing observations in kinetically constrained models. Our results here illustrate the applicability of exact tensor network methods for solving problems in many-body stochastic systems.

---

* This paper is dedicated to the memory of Marko Medenjak (1990–2022).
** Author to whom any correspondence should be addressed.

1. Introduction

Kinetically constrained models (KCMs, for reviews see [1, 2]) are stochastic lattice systems used to describe the slow dynamics of glass formers [3–5]. They furnish the idea [6, 7] that slow dynamics, as seen in supercooled liquids and other glassy systems, is not a consequence of an underlying singular change in thermodynamics but of effective constraints in the dynamics. While the natural description of a liquid is that of a hard sphere system with continuous degrees of freedom, the basic thinking motivating KCMs [8–10] is that under supercooled conditions (low temperature and/or high density) an effective description in terms of a KCM with discrete degrees of freedom is obtained by coarse-graining small space and short time features in the liquid. The resulting system retains the key physical property of local steric constraints that gives rise to slow cooperative relaxation. Out of the whole class of KCMs, the East model [11] is particularly important as its hierarchical relaxation properties [12] allow to explain [9, 10, 13] many phenomenological features of the glass transition. Since KCMs have simple thermodynamics but complex dynamics, it is natural to study them through the statistical properties of their stochastic trajectories [14], specifically via dynamical large deviation (LD) methods [5, 15–18].

In [19] we proved via exact methods that a system we called the 'deterministic Floquet-East (DFE) model' exhibits a first-order phase transition in its dynamical large deviations, and as consequence it displays dynamical fluctuations corresponding to pre-transition behaviour, a dynamical equivalent of the hydrophobic effect in water [20, 21]. Defined in terms of a discrete-space/discrete-time circuit with a 'brickwork' arrangement of local deterministic (i.e. permutation) gates, the DFE [19] (see also [22–25]) is a deterministic generalisation (and simplification) of the East model (whose dynamics is stochastic and continuous in time), with the two models sharing the same kinetic constraint. The standard East model exhibits a phase transition at the trajectory level where the order parameter is the dynamical activity, an observable counting the number of configuration changes [16, 26, 27]. This is a first-order transition between two dynamical phases, an ergodic equilibrium and dynamically active phase, and a non-ergodic inactive phase. While the dynamics is at coexistence in the limit of infinite time, for any finite observation time the large majority of initial conditions favour the active phase, so that without biasing the typical dynamics of the East model is ergodic, and the corresponding stationary state is a featureless product state. Despite that, the existence of the inactive phase has profound consequences: even in ergodic trajectories mesoscopic fluctuations of inactivity (or 'space-time bubbles') are predominant, giving rise to dynamic heterogeneity and glassy relaxation [5, 6, 28]. These fluctuations are a dynamical analogue of those that give rise to hydrophobic physics in liquid water [29], since the physical origin is the proximity to a first-order transition (i.e. a dynamical instance of the *orderphobic effect* [30], where all that matters is the proximity to a coexistence of phases, irrespective of whether the associated transition is an equilibrium or a non-equilibrium one).

The results of [19] for the DFE were obtained via exact tensor network methods similar to those being currently used to solve certain cellular automata, see e.g. [22, 31–42], or quantum circuits, see e.g. [24, 25, 43–60]. The dynamics of the DFE model displays an analogous active-inactive large deviation transition and corresponding dynamical 'hydrophobic' fluctuations as the standard East model, which suggests that the origin of this kind of physics is the local kinetic constraint that both models share. However, one might wonder if the deterministic nature of the DFE means that there is a fundamental difference between the two models, and that the exact results obtained in the DFE are not informative of what happens when stochasticity is present. In this paper we resolve this question.
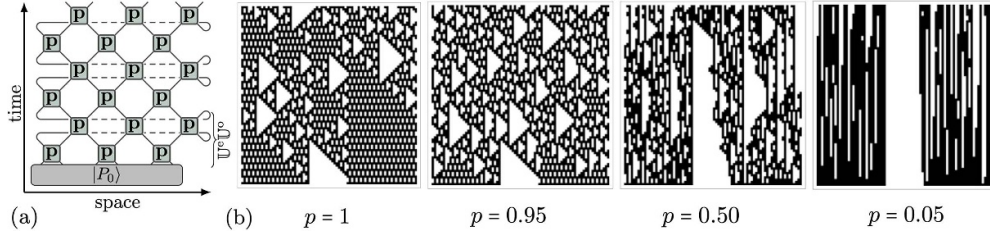
Figure 1. Stochastic Floquet-East model. (a) Diagrammatic representation of time-evolution in a finite system with periodic boundary conditions. The dashed line represents the connection between the left and right edge. (b) Examples of trajectories initialised in the same domain-wall state $|P_0\rangle = |1\rangle^{\otimes 2L/5} \otimes |0\rangle^{\otimes L/5} \otimes |1\rangle^{\otimes 2L/5}$ for $L = 100$ and several values of p. States zero/one are represented by white/black dots.

We consider a stochastic generalisation of the DFE, or *stochastic Floquet-East* model. Like its deterministic counterpart, the stochastic Floquet-East is defined as a discrete brickwork circuit (see figure 1(a) for a diagrammatic representation) with the same East model kinetic constraint, that is, a site can only flip if its nearest neighbour 'to the East' is in the excited state. However, the main difference in the stochastic model is that flips only occur with a certain probability. Using exact tensor network methods we: (i) prove that in the long time and large size limit the stochastic Floquet-East also has a large deviation phase transition between active and inactive dynamical phases; (ii) compute the finite time and size scaling of space-time fluctuations, showing that inactive space-time regions gives rise to dynamical hydrophobicity; (iii) show that the results of the DFE bound those of the stochastic Floquet-East; and (iv) demonstrate that our results for the stochastic Floquet-East also hold for the standard continuous-time East model in an appropriate 'Trotter' limit, thus proving long-standing observations in kinetically constrained models.

The rest of the paper is organised as follows. In section 2 we introduce the model. In section 3, by studying the large deviations of the activity, we prove the existence of a transition between active and inactive phases, and show that these results also extend to an appropriate limit to the standard continuous-time East model. In section 4 we consider the statistics of finite inactive space-time regions, and show the emergence of dynamical pre-transition (or 'hydrophobic') effects. In section 5 we compute the statistics of arbitrary finite space-time arrangements, and we show how these are different from to those of inactive space-time regions. We give our conclusions and outlook in section 6.

2. Stochastic Floquet-East model

The model is defined on a lattice of $2L$ sites of binary variables $n_i \in \{0,1\}$ with periodic boundaries, where lattice sites are labelled by half-integer values, $i \in \{\frac{1}{2}, 1, \ldots, L - \frac{1}{2}, L\}$. The statistical states $|P\rangle$ are probability distributions over the finite set of all configurations $\mathbf{n} = (n_{\frac{1}{2}}, n_1, \ldots, n_{L-\frac{1}{2}}, n_L)$,

$$|P\rangle = \sum_{\mathbf{n}} P(\mathbf{n}) |n\rangle, \qquad P(\mathbf{n}) \geqslant 0, \qquad \sum_{\mathbf{n}} P(\mathbf{n}) = \langle -|P\rangle = 1, \qquad (1)$$

where $|n\rangle = |n_{\frac{1}{2}}\rangle \otimes \cdots \otimes |n_L\rangle$. The state $\langle -| = \sum_{\mathbf{n}} \langle \mathbf{n}|$, also called *flat state*, describes the unnormalized uniform distribution. The time-descrete dynamics, shown in figure 1(a), consists

of two distinct steps,

$$|P_{t+1}\rangle = \mathbb{U}^{\text{e}}|P_{t+\frac{1}{2}}\rangle = \mathbb{U}^{\text{e}}\mathbb{U}^{\text{o}}|P_t\rangle, \qquad t \in \mathbb{Z}. \tag{2}$$

Note that time is also labelled by half-integer numbers. The time-evolution operators $\mathbb{U}^{\text{o/e}}$ consist of mutually commuting nearest-neighbour updates,

$$\mathbb{U}^{\text{e}} = U_p^{\otimes L}, \qquad \mathbb{U}^{\text{o}} = \Pi_L U_p^{\otimes L} \Pi_L^{\dagger}, \tag{3}$$

where Π_L is a one-site shift operator, and U_p the 4×4 matrix implementing the two-site update

$$\langle m'n'|U_p|mn\rangle = \delta_{n',0}\delta_{n,0}\delta_{m',m} + \delta_{n',1}\delta_{n,1}\left[\delta_{m',1-m}p + \delta_{m',m}\left(1-p\right)\right], \tag{4}$$

with $|mn\rangle = |m\rangle \otimes |n\rangle$. The above matrix encodes the kinetic constraint: if the right site is in state one, the spin on the left site changes with fixed probability $0 \leqslant p \leqslant 1$, and stays the same otherwise.

Throughout the paper we will make use of the diagrammatic tensor network notation [61], where tensors are represented by nodes (or vertices) with lines emanating from them. The number of lines corresponds to the rank of the tensor, and lines connecting two nodes indicating a contraction along that dimension. For example, in this representation local vectors corresponding to one physical site are

$$\underset{\textcircled{v}}{\big|} = |v\rangle = v_0\,|0\rangle + v_1\,|1\rangle, \qquad \underset{0}{\big|} = |0\rangle, \qquad \underset{1}{\big|} = |1\rangle, \qquad \perp = \underset{0}{\big|} + \underset{1}{\big|} = |-\rangle, \tag{5}$$

where we introduced a shorthand notation for computational-basis states, and the one-site flat state $|-\rangle$. In this language a free line represents a one-site identity matrix, and the inner product is given by contracting two vectors,

$$\langle w|v\rangle = \underset{\textcircled{v}}{\overset{\textcircled{w}}{\big|}}, \qquad \big| = \begin{bmatrix} 1 & 0 \\ 0 & 1 \end{bmatrix}. \tag{6}$$

We introduce a green box with 4 legs to represent the tensor which, when interpreted as acting upwards, gives U_p,

$$\underset{m \quad n}{\overset{m' \quad n'}{\boxed{\mathbf{P}}}} = \langle m'n'|U_p|mn\rangle. \tag{7}$$

Using these conventions, the full time-evolution can be represented as the tensor network shown in figure 1(a). In the limiting cases of $p = 1$ or $p = 0$ the dynamics becomes deterministic, corresponding to the DFE model [19, 24] and trivial (identity) dynamics, respectively,

$$\boxed{\mathbf{1}} =: \boxed{}, \qquad \boxed{\mathbf{0}} = \big) \big(. \tag{8}$$

Figure 1(b) shows some typical trajectories for systems prepared in the same domain-wall initial state at different values of p. For $p = 1$ (the DFE case), trajectories are characterised by the presence of stationary space-time regions of triangular shape. These empty regions can be still observed away from the deterministic limit, $0 < p < 1$, but since flips are stochastic these regions are not necessarily triangular and may be much more extended in time than in the deterministic case. The similarities between trajectories in the stochastic East model and the standard East model [28] are evident: despite dynamics being ergodic overall, there

is a preponderance of dynamical fluctuations, with slow inactive 'bubbles' punctuated by the sudden onset of activity which leads to overall relaxation[4].

For later convenience, we define the *tilted* gate $U_{p,s}$, where each time the spin-flip occurs, we introduce a factor of e^{-s}, which we represent by a dark-shaded box,

$$U_{p,s} = \begin{bmatrix} 1 & & & \\ & 1-p & e^{-s}p & \\ & & 1 & \\ & e^{-s}p & & 1-p \end{bmatrix}, \qquad \begin{matrix} m' & n' \\ \boxed{\text{p}} \\ m & n \end{matrix} = \langle m'n'|U_{p,s}|mn\rangle, \qquad \boxed{\text{p}} = \boxed{\text{p}} + e^{-s}\boxed{\text{p}}. \tag{9}$$

Here, the blue and red squares are the *inactive* and *active* parts of the gate (i.e. they include the matrix elements with no-flips and flips respectively). By inspecting their matrix elements, we immediately note that the inactive gate factorizes into an identity on the left, and a diagonal transformation on the right site,

$$\boxed{\text{p}} =) \langle, \qquad \phi = \begin{bmatrix} 1 & 0 \\ 0 & 1-p \end{bmatrix}, \tag{10}$$

while the active gate is the same as the active gate in the $p=1$ case multiplied by a factor of p,

$$\boxed{\text{p}} = p\ \blacksquare, \qquad \begin{matrix} m' & n' \\ \blacksquare \\ m & n \end{matrix} = \delta_{m,1-m'}\delta_{n,1}\delta_{n',1}. \tag{11}$$

Apart from the diagonal transformation introduced in (10), we will make use two other one-site observables: a projector to the zero and one state, respectively represented by a white and black circle,

$$\phi = \begin{bmatrix} 1 & 0 \\ 0 & 0 \end{bmatrix}, \qquad \bullet = \begin{bmatrix} 0 & 0 \\ 0 & 1 \end{bmatrix}. \tag{12}$$

The model is bi-stochastic, that is, both the dynamics and its inverse conserve probability, which is a consequence of the flat state being both a left and right eigenvector of the local time-evolution operator

$$U_p|-\rangle \otimes |-\rangle = |-\rangle \otimes |-\rangle, \qquad \langle-| \otimes \langle-|U_p = \langle-| \otimes \langle-|. \tag{13}$$

These two local relations can be equivalently represented using the above graphical language as

$$\boxed{\text{p}} =) (, \qquad \boxed{\text{p}} =) (. \tag{14}$$

Moreover, the gates exhibit a stronger property: whenever one acts with a flat state from either top or bottom on the *left* site, it factorizes into a projector to the flat state and an identity operator,

$$\boxed{\text{p}} =) (, \qquad \boxed{\text{p}} =) (, \tag{15}$$

---

[4] While the activity 'avalanches' can be seen as reminiscent of those in non-equilibrium setups such as self-organised criticality [65], for KCMs such as the East model they correspond to spontaneous (and non-critical) fluctuations that occur in the equilibrium dynamics.
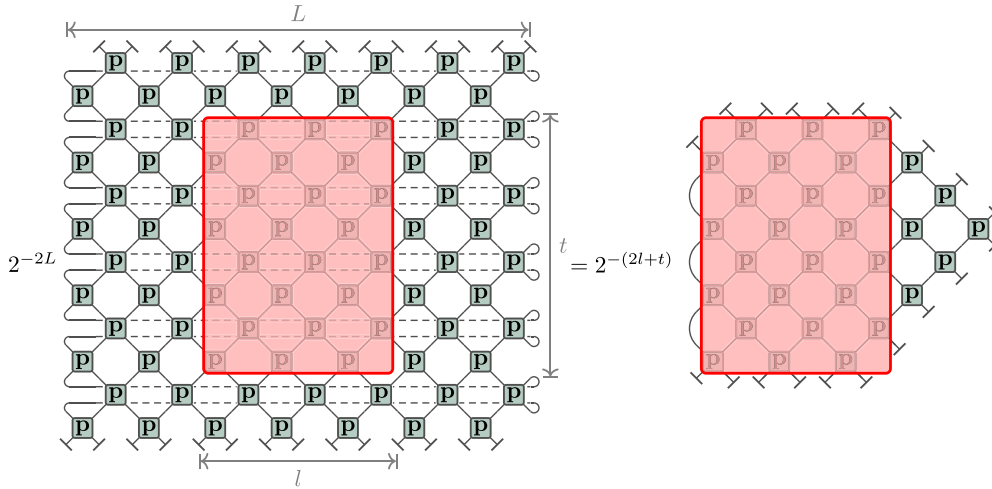
Figure 2. Local correlations and expectation values in a space-time box embedded in a large system. The l.h.s. shows a schematic representation of an infinite-temperature correlation function between observables that are confined to a space-time box of sizes $l \times t$ (represented by the red rectangle), embedded in a larger system of size L with periodic boundary conditions. As long as $l + t < L$, we can repeatedly apply local relations in equations (14) and (15) to recast the object as the same correlation function (represented by the red box), but now evaluated in a finite system with special boundary conditions (r.h.s.), see appendix for details. Note that the size of the green triangle on the r.h.s. scales with time t.

which can be understood as a stochastic analogue of the generalization of dual unitarity introduced in [63], but here it only applies to one side. This property implies that an invariant state of the space-evolution coming from the left consists of dimer product states, as shown in figure 2(see also appendix). We note that for $p = 1$ the gates preserve flat states coming from the right, which implies a simple form also for the invariant states under space evolution from right to left [19], but this ceases to hold for generic p.

3. Dynamical large deviations

As is proven in [19], the DFE model exhibits a first-order phase transition between and 'active' and an 'inactive' dynamical phase—phases with a large and small number of spin flips, respectively. Below, we show that the same is true for the stochastic generalisation.

We consider a space-time region of size $l \times t$ in a much larger system of size $L \times T$, and we take the dynamical order parameter to be the dynamical activity—total number of spin flips in the region $l \times t$. Let $\{\omega\}$ be the set of all the possible trajectories in the full system, $\pi_p(\omega)$ probability of the trajectory ω, and $K_{l,t}(\omega)$ its activity. Then the moment generating function of the activity is given by [15, 17, 18]

$$Z_{l,t}(p,s) = \sum_{\omega} \pi_p(\omega) e^{-sK_{l,t}(\omega)}, \tag{16}$$

where we will assume that the initial configuration is uniformly distributed. Equivalently, $Z_{l,t}(p,s)$ can be interpreted as a partition function for a *tilted region* [i.e. a region where the

stochastic gates U_p are replaced by tilted gates (9)] of size $l \times t$ embedded in a much larger system of size $L \times T$, which can be diagrammatically represented as

$$Z_{l,t}(s) = 2^{-(2l+t)} \quad t \quad \text{[diagram]} \quad . \tag{17}$$

The contraction that leads from the large space-time region $L \times T$ to the above diagram has been obtained by using relations (14) and (15) and by following the procedure described in figure 2. Though conceptually simple, the diagram in equation (17) cannot be evaluated exactly for all s. However, we are able to bound the behaviour effectively in two limits, $s \approx 0$, and $s \to \infty$, which—upon evoking general properties of the moment generating function $F_{l,t}(p,s) = \log Z_{l,t}(p,s)$—suffices to demonstrate the existence of a first-order phase transition.

3.1. Expansion around $s \approx 0$

The first regime of interest is $s \approx 0$, where $Z_{l,t}(p,s)$ is well approximated by the expansion up to s^2,

$$Z_{l,t}(p,s) \approx 1 - s Z_{l,t}^{(1)}(p) + s^2 Z_{l,t}^{(2)}(p) + \mathcal{O}(s^3), \tag{18}$$

where we took into account that the bi-stochasticity (14) implies $Z_{l,t}(p,0) = 1$. By expanding each of the tilted gates as

$$\text{[diagram]} = \text{[diagram]} + (e^{-s} - 1)\,\text{[diagram]}, \tag{19}$$

one sees that in the first-order the contribution is given in terms of one-point functions in the stationary state, which can be easily evaluated as

$$Z_{l,t}^{(1)}(p) = \sum_{\{x,y\}} 2^{-(2l+t)} \quad \text{[diagram]} \quad = \sum_{\{x,y\}} \frac{1}{4}\,\text{[diagram]} = plt, \tag{20}$$

where the sum goes over all positions $\{x,y\}$ inside the rectangular part [i.e. the shaded part in (17)]. The first equality above, again, follows directly from the bi-stochasticity, and the final

result from the definition of the gate. The second-order correction requires some more work, as now we get contributions both from the one and two-point functions,

$$Z_{l,t}^{(2)}(p) = \frac{1}{2} Z_{l,t}^{(1)}(p) + \frac{1}{2} \sum_{\{x_1,y_1\} \neq \{x_2,y_2\}} p^2 2^{-(2l+t)} \underbrace{\qquad\qquad\qquad}_{C_2(\{x_1,y_1\},\{x_2,y_2\};p)}. \tag{21}$$

Using the observation

$$\boxed{p} = \quad , \qquad \boxed{p} = \quad , \tag{22}$$

and explicitly treating the case $\{x_2,y_2\} = \{x_1,y_1\} + \{\pm 1, \pm 1\}$, one can show that whenever $x_1 \neq x_2$ the correlation function factorizes,

$$C_2(\{x_1,y_1\},\{x_2,y_2\};p)\big|_{x_2 \neq x_1} = \left(\frac{1}{4} \boxed{p}\right)^2 = \frac{p^2}{4}. \tag{23}$$

When $x_1 = x_2$, however, the two-point correlation function no longer factorizes, but instead depends on the distance between the two points, $|y_2 - y_1|$, which can take only positive integer values between 1 and $t - 1$,

$$C_2(\{x,y\},\{x,y \pm m\};p) = 2^{-(m+2)} \; m \; \boxed{\qquad} = p^2 2^{-(m+1)} \; m-1 \; \boxed{\qquad} = p^2 c_2(p,m-1), \tag{24}$$

where we introduced the short-hand notation $c_2(p,m)$ in terms of which the full second-order contribution reads as

$$Z_{l,t}^{(2)}(p) = \frac{plt}{2} + \frac{p^2}{4} lt(2lt-1) + 2lp^2 \sum_{m=0}^{t-2} \left(c_2(p,m) - \frac{1}{4}\right). \tag{25}$$

We are not able to evaluate $c_2(p,m)$ exactly, however, we are able to provide some bounds on its magnitude. We start by noting that it can be understood as a matrix element

$$c_2(p,m) = \frac{1}{2} \begin{bmatrix} 0 & 1 \end{bmatrix} R_m(p) \begin{bmatrix} 0 \\ 1 \end{bmatrix}, \qquad R_m(p) = 2^{-(m+1)} \ m \ \left| \ \right. \tag{26}$$
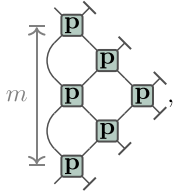
where $R_m(p)$ denotes the matrix between the free legs on bottom and top. As individual gates comprising $R_m(p)$ are bi-stochastic matrices, also $R_m(p)$ is bi-stochastic, therefore there exists a m and p-dependent value $r_m(p)$ so that

$$0 \leqslant r_m(p) \leqslant 1, \qquad R_m(p) = \begin{bmatrix} r_m & 1-r_m \\ 1-r_m & r_m \end{bmatrix}. \tag{27}$$

Expressing $c_2(p,m)$ in terms of r_m we obtain both a lower and an upper bound,

$$0 \leqslant c_2(p,m) = \frac{1}{2} r_m \leqslant \frac{1}{2}, \tag{28}$$

with the lower bound $c_2(p,m) \geqslant 0$ being trivial, as it follows directly from non-negativity of the matrix elementes. However, the upper bound is tight, since it is saturated for $p = 0$,

$$c_2(p,m) \leqslant \frac{1}{2} = c_2(0,m). \tag{29}$$

Using these, we can bound the second order contribution as

$$\frac{(plt)^2}{2} + \frac{plt}{4}\left(2 - p\left(3 - \frac{2}{t}\right)\right) \leqslant Z_{l,t}^{(2)}(p) \leqslant \frac{(plt)^2}{2} + \frac{plt}{4}\left(2 + p\left(1 - \frac{2}{t}\right)\right). \tag{30}$$

This is enough to understand the asymptotics of $Z_{l,t}^{(2)}$: in the limit of $l,t \to \infty$ with l/t fixed, the leading order contribution is $(plt)^2/2$, with the precise form of $c_2(p,m)$ determining the subleading term.

3.2. $s \to \infty$ limit

Let us proceed by considering the $s \to \infty$ limit of $Z_{l,t}(p,s)$. We start by noticing that the stochastic generalized inactive gate, when seen as evolving in time, acts on the two sites as

a product of an identity and a diagonal transformation respectively, as shown in equation (10). Using this representation of the gate we can express the partition sum as

$$
\lim_{s\to\infty} Z_{l,t}(p,s) = 2^{-(2l+t)}\ \ \ \ = 2^{-(2l-1+t)}\left[1+(1-p)^t\right]^{2l-1}
$$

(31)

$$
=: \left(\frac{1+(1-p)^t}{2}\right)^{2l-1} T_t(p),
$$

where we introduced $T_t(p)$ to denote the value of the triangular diagram on the right multiplied by 2^{-t}. Analogously to before, we are not able to exactly evaluate $T_t(p)$ for generic p, but we can straightforwardly bound it from above and below by its values in the two deterministic points, $T_t(0)$ and $T_t(1)$. The lower bound is obtained by using the positivity of p and $1-p$ to show

$$
T_t(p) \geq 2^{-t}\ \ \ \ = 2^{-t} = T_t(1).
$$

(32)

To find the upper bound we use that the diagonal transformation in (10) together with the projector to the state 1 sum up to the identity,

$$
\ \ + p\ \ = \ ,
$$

(33)

which—together with the positivity of all the entries of the local gate—gives

$$
T_t(p) \leq 2^{-t}\ \ \ \ = 1 = T_t(0).
$$

(34)

In summary, we have the following bounds on the p-dependent partition sum,

$$
2^{-t}\left(\frac{1+(1-p)^t}{2}\right)^{2l-1} \leqslant \lim_{s\to\infty} Z_{l,t}(p,s) \leqslant \left(\frac{1+(1-p)^t}{2}\right)^{2l-1}.
$$

(35)

In particular, this means that the partition sum in the $s \to \infty$ limit is in general larger than at $p = 1$,

$$\lim_{s \to \infty} Z_{l,t}(p,s) \geqslant \lim_{s \to \infty} Z_{l,t}(1,s). \tag{36}$$

The above bounds hold for any p, and are tight, since they are saturated by the two deterministic limits of the model. However, we can find an alternative lower bound that is tighter for $p \leqslant \frac{1}{2}$. By decomposing the transformation (10) as

$$\phi = (1-p)\Big| + p\, \Diamond, \tag{37}$$

we have

$$T_t(p) \geqslant (1-p)^t T_t(0) = (1-p)^t. \tag{38}$$

This gives

$$\lim_{s \to \infty} Z_{l,t}(p,s) \geqslant \left(\frac{1 + (1-p)^t}{2} \right)^{2l-1} (1-p)^t. \tag{39}$$

3.3. Phase transition in the dynamical large deviations

The occurrence of the phase transition is a consequence of different scaling of $Z_{l,t}(p,s)$ with the subregion size in the two limits. To show this, we define the cumulant generating function $F_{l,t}(p,s)$, and its asymptotic value $F(p,s)$ as

$$F_{l,t}(p,s) = \frac{1}{lt} \log Z_{l,t}(p,s), \qquad F(p,s) = \lim_{l \to \infty} F_{l,l\xi}(p,s), \tag{40}$$

where we introduced ξ to represent the asymptotic ratio between the two sizes of the space-time region, $\xi = t/l$. Plugging in the results above we have a well-behaved expansion around $s \approx 0$,

$$F(p,s) = -ps + \frac{1}{2}ps^2(1+A_p) + \mathcal{O}(s^3), \qquad -\min\left\{1, \frac{3p}{2}\right\} \leqslant A_p \leqslant \frac{p}{2}, \tag{41}$$

where we introduced A_p to denote a p-dependent constant that we can bound as shown above. On the other hand, in the limit $t \to \infty$ the rescaled cumulant generating function vanishes,

$$\lim_{s \to \infty} F(p,s) = 0. \tag{42}$$

We now note that for finite l,t by definition $F_{l,t}(p,s)$ is analytic and *convex* [17]. Combining this with the above asymptotic scaling we have that in the thermodynamic limit the first derivative must become discontinuous, and the model exhibits a first-order phase transition.

3.4. Trotter limit

In the appropriate scaling limit of large *t* and small *p*, the stochastic Floquet-East model reproduces the dynamics of the standard continuous-time stochastic East model [1, 11]. Interestingly, the above argument carries over to this limit as well.

We start by introducing the continuous-time partition sum $\mathcal{Z}_{l,t}(\Gamma,s)$, where *t* now denotes *real time* (and not the number of time-steps), *l* is as before the size of the subsystem of interest, and Γ is the rate with which the spins in the continuous-time model flip. The dynamics of the continuous-time model is approximated by the stochastic Floquet-East when for a small Δ we scale the number of time-steps as t/Δ, while the probability parameter goes as $\Delta\Gamma$. This gives the following continuous-time limit of the partition sum

$$\mathcal{Z}_{l,t}(\Gamma,s) = \lim_{\Delta\to 0} Z_{l,\frac{t}{\Delta}}(\Gamma\Delta,s). \tag{43}$$

Using the small-*s* expansion of the discrete-time partition sum we get,

$$\mathcal{Z}_{l,t}(\Gamma,s) = 1 - s\Gamma lt + s^2 \frac{lt\Gamma}{2}(1 + lt\Gamma) + \mathcal{O}\left(s^3\right), \tag{44}$$

where we used that the upper and lower bounds in equation (30) coincide in the Trotter limit, and give us an exact expression. Similarly, we can plug-in the $s\to\infty$ bounds to obtain

$$e^{-\Gamma t}\left(\frac{1+e^{-\Gamma t}}{2}\right)^{2l-1} \leq \lim_{s\to\infty}\mathcal{Z}_{l,t}(\Gamma,s) \leq \left(\frac{1+e^{-\Gamma t}}{2}\right)^{2l-1}. \tag{45}$$

Note that here we need to use the lower bound given by equation (39), since for small *p* it is stricter than that of equation (35).

We now have all the ingredients to understand the scaling of the thermodynamic-limit of the continuous-time cumulant generating function,

$$\mathcal{F}(\Gamma,s) = \lim_{l,t\to\infty}\frac{1}{lt}\log\mathcal{Z}_{l,t}(\Gamma,s). \tag{46}$$

As before, for small *s* it has a well-behaved expansion around 0, while it goes to zero for $s\to\infty$.

$$\mathcal{F}(\Gamma,s)|_{s\approx 0} = -\Gamma s + \frac{s^2}{2}\Gamma + \mathcal{O}\left(s^3\right), \qquad \lim_{s\to\infty}\mathcal{F}(\Gamma,s) = 0, \tag{47}$$

therefore our results prove the existence of the phase transition also in the Trotter limit.

4. Distribution of empty space-time regions

We now consider the probability $P_\square(l,t;p)$ of finding an empty region of size $l\times t$ within the dynamics, see figure 3(a) for a precise definition. In particular, we want to study how the probability scales for large sizes. We assume *l* and *t* to be integer numbers for simplicity, however, generalisations to semi-integers follow naturally, and do not change the scaling. In [19], the above probability has been computed in the deterministic limit when $p = 1$ and gives

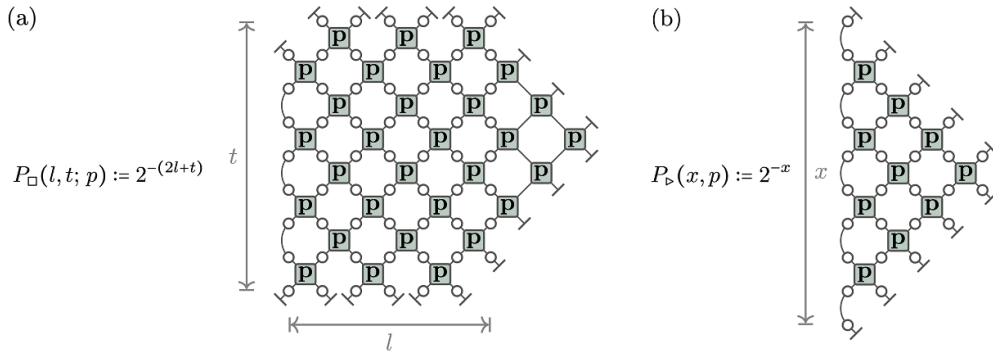$$P_\square(l,t;1) = \frac{1}{2}\lim_{s\to\infty} Z_{l,t}(1,s) = 2^{-(2l+t)}. \tag{48}$$

Figure 3. (a) Probability of finding a region of states zero within a box of size $l \times t$. (b) Probability of finding a region of states zero within a equilateral triangle with base being of length x.

Thus, the probability $P_\square(l,t;1)$ manifestly scales with perimeter. Furthermore, a rectangular condition of emptiness such as the one displayed in figure 3(a) implies a larger triangle surrounding the box to be all in states zero. As a consequence we have the following equality,

$$P_\square\left(l,t;1\right) = P_\triangleright\left(2l+t,1\right), \tag{49}$$

where $P_\triangleright$ is the probability of finding an empty region of triangular shape, see figure 3(b) for definition in the stochastic model. In particular, the identity

directly implies that the probability of an empty triangle does not depend on p,

$$P_\triangleright\left(x,p\right) = 2^{-x} = P_\triangleright\left(x,1\right). \tag{51}$$

We need to stress that equation (49) is a special property of the DFE model and no longer holds for $p \neq 1$, even though the probability of a triangular hole does not depend on the precise value of p. In particular, repeating the reasoning leading to (51), one obtains the following expression for the probability of a rectangular empty region for a generic value of p,

with the r.h.s. straightforwardly following from the definitions (10). The above partition sum is typically hard to evaluate for general $t \in \mathbb{N}$, as the blue circles account for the stochastic behaviour of the system, and the resulting graph is a complicated polynomial function of p.

13

However, it can be bounded by the two deterministic limits through the very same argument presented above equation (34):

$$P_\square(l,t;1) = 2^{-2l-t} \leqslant P_\square(l,t;p) \leqslant 2^{-2l-1} = P_\square(l,t;0) . \tag{53}$$

It follows that the probability $P_\square(l,t;p)$ can *at most* scale with perimeter, and the triangular fluctuations characterising the DFE model provide a lower bound for the stochastic probabilities.

The result in equation (53) is an analytic proof that the stochastic Floquet East model displays *dynamic hydrophobicity*. While the much studied hydrophobic effect in water is a purely static phenomenon, it originates from the first-order nature of water's liquid-vapour transition [20, 21]. The insight of [30] was that other systems with first-order transitions should display similar pre-transition physics, leading to the generic *orderphobic effect*. However, this observation is not limited to thermodynamics. When going from statics to dynamics, one moves from considering ensembles of configurations to *ensembles of trajectories*, with the moment generating function (16) being the partition sum over trajectories. Since, as proved in section 3.3 above, the DFE has a first-order dynamical transition between active and inactive phases, the results in this section demonstrate the accompanying pre-transition effects, in analogy to what occurs in static problems, i.e. a dynamical version of the hydrophobic (or orderphobic) effect. Furthermore, given that our stochastic Floquet East model is related to the standard East model via Trotterisation, see section 3.4, our exact results here validate previous numerical observations of pre-transition physics in that model [29].

5. Distribution of generic space-time trajectories

One may wonder if the results of section 4 can be generalised to more general trajectories, and whether a probability of observing an empty region is somehow special compared to probabilities of observing more general space-time configuration. To address this question, we introduce the probability $P(\tau(l,t);p)$ of finding a particular trajectory $\tau(l,t)$ inside a box of size $l \times t$. In the deterministic case, the probability $P(\tau(l,t);1)$ equals the probability of having an empty region of the same size, provided that the trajectory $\tau(l,t)$ is allowed by the dynamics. We illustrate this by considering, for instance, a horizontal line of finite length l of a random combination of states zero and one. The corresponding probability is

$$P(\tau(l,1/2);1) = 2^{-L} \qquad = 2^{-L} \qquad = 2^{-2l} \qquad = P_\triangleright(2l) . \tag{54}$$

The above result reproduces the probability of finding an empty triangle of base $2l$ in equation (51). Through equations (49) and (54), we can more generally say that the probability

14

$P(\tau(l,t);1)$ of finding a box of size $l \times t$ in a particular (deterministic) trajectory $\tau(l,t)$ is

$$P(\tau(l,t);1) = \begin{cases} P_\square(l,t;1) & \text{for any allowed trajectory } \tau(l,t), \\ 0, & \text{otherwise}. \end{cases} \quad (55)$$

Therefore the empty regions are not particularly special in the deterministic case, and any allowed trajectory scales with perimeter.

The above statement no longer holds for the stochastic dynamics, where the probability $P(\tau(l,t);p)$ strongly depends on the choice of trajectory $\tau(l,t)$. Indeed we can easily find trajectories $\tau(l,t)$ for which the corresponding probabilities $P(\tau(l,t);p)$ scale with area rather than perimeter, these include trajectories forbidden by the deterministic dynamics such as the space-time region including all states one. The corresponding probability is:

$$P_\blacksquare(l,t;p) = 2^{-(2l+t)} \; \cdots \; = (1-p)^{2lt}\, 2^{-(2l+t)} \; \cdots \; = (1-p)^{2lt}\, P_\square(l,t;p), \quad (56)$$
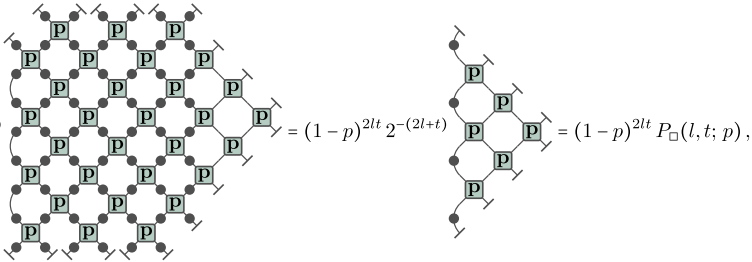
where $P_\square(l,t;p)$ is given by (52). To arrive to the second and third equality we respectively used the following two observations,

$$\cdots = (1-p) \; \cdots \; , \qquad \cdots = \cdots . \quad (57)$$
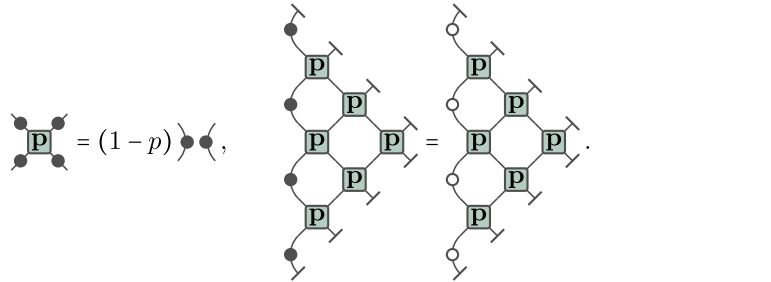
In particular, equation (56) implies that the probability $P_\blacksquare(l,t;p)$ scales with area for any $p \neq 1$ and large l and t. Note that the result above holds for any trajectory forbidden by the deterministic dynamics—i.e. any trajectory for which we have $P(\tau(l,t);1)=0$.

Let us now consider the probability of a generic trajectory $\tau(l,t)$, such as the following,

$$P(\tau(l,t);p) = 2^{-(2l+t)} \; \cdots \; . \quad (58)$$
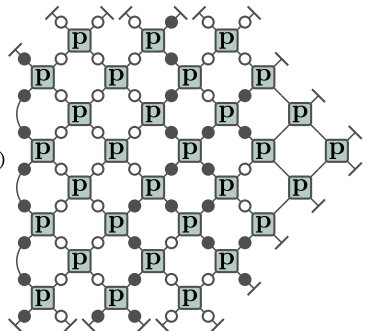
The above probability always factorises into two contributions, $P_1(\tau(l,t);p)$ and $P_2(\tau(l,t);p)$, scaling with area and perimeter, respectively. Our particular example can be rewritten as

$$P(\tau(l,t);p) = P_1(\tau(l,t);p) \; 2^{-(2l+t)} \; \underbrace{\quad\quad\quad\quad\quad}_{P_2(\tau(l,t);p)} . \tag{59}$$
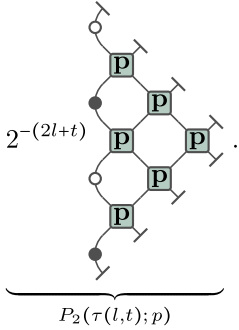
where $P_1(\tau(l,t);p)$ and the line of projectors onto zero and one in the first column of $P_2(\tau(l,t);p)$ are straightforwardly determined by the trajectory within the box. In particular, we have that

$$P_1(\tau(l,t);p) = p^K (1-p)^{2lt-K-J} , \tag{60}$$

where $K := K(\tau(l,t))$ is the number of spin flips, and $J := J(\tau(l,t))$ is the number of all the gates where the right spins are in the 0 state (i.e. all the gates that would not flip in the $p=1$ limit). On the other hand, $P_2(\tau(l,t);p)$ can be bounded by using the following inequalities,

$$2^{-t} \quad\quad \leq 2^{-t} \quad\quad \leq 2^{-t} \quad\quad = 1 . \tag{61}$$
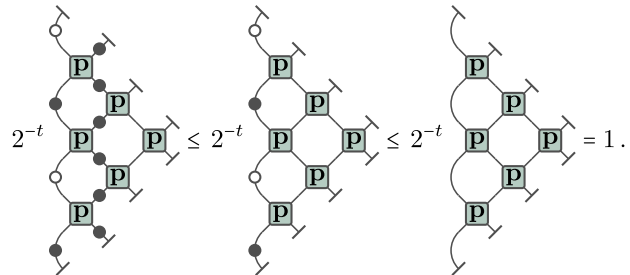
Above, the rightmost graph represents the sum over all the possible trajectories within the triangle, while the leftmost graph is the sum over the fewer trajectories of the central graph conditioned to having all ones in the second column. Note that the inequalities above can be generalised for any allowed trajectories and will always reproduce a non-trivial lower bound, provided that $p \neq 0, 1$. Moreover, we can express the leftmost graph as

$$2^{-t} \quad\quad = 2^{-t} p^{t-1/2-y} (1-p)^y \quad\quad = 2^{2l-1} p^{t-1/2-y} (1-p)^y P_\square(l, t-1; p) , \tag{62}$$
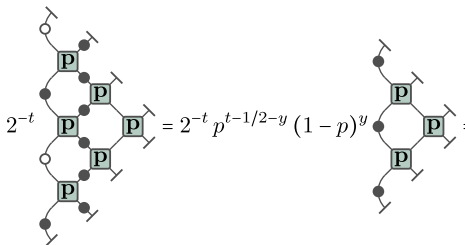
and the power $0 \leqslant y \leqslant t$ depends on the particular trajectory. Thus, the inequalities in equation (61) can be rewritten as

$$\frac{p^{t-1/2-y}(1-p)^y}{2} P_\square(l, t-1; p) \leqslant P_2(\tau(l,t); p) \leqslant 2^{-2l}. \tag{63}$$

As a result, $P_2(\tau(l,t); p)$ is at most exponential in l and t, and thus scales with perimeter. In contrast, the area-dependence comes from $P_1(\tau(l,t); p)$, which can be written as:

$$P_1(\tau(l,t); p) = 2^{-\frac{2lt}{\log 2}(k \log p + (1-k-j)\log(1-p))}. \tag{64}$$

where $k = K/2lt$ and $j = J/2lt$ are the densities of k amd j respectively. The dominant contribution can be related to the density of zero in the trajectory: we have that $P(\tau(l,t); p)$ scales with perimeter i.e. $P_1(\tau(l,t); p) \sim 1$ whenever empty regions dominate the trajectory i.e. $j \sim 1$ and $k \sim 0$, while it scales with area in any other case.

6. Conclusions

In this paper, we have introduced and studied via exact tensor network methods a stochastic generalisation of the classical deterministic Floquet-East model. We proved that, just like the standard East model [16, 27] or the deterministic Floquet-East [19], with which it shares the local constraint of spin flips only allowed in the vicinity of an excited nearest neighbours to one side (say, to the left or East side), the stochastic Floquet-East model has a phase transition at the large deviation level between an active and ergodic dynamical phase and an inactive and non-ergodic dynamical phase. This dynamical transition is first-order, meaning that even in the ergodic phase (favoured by the vast majority of initial conditions) there are pronounced finite (in space and time) fluctuations of inactivity that correspond to pre-transition effects: for large enough inactive 'bubbles' their log probability scales with perimeter and not area, since it is more favourable to create a domain of the inactive phase, paying only an interface cost. This is the same physics in space-time of the celebrated hydrophobic effect in water [20, 21] or the more general orderphobic effect [30]. We also showed that in an appropriate limit the stochastic Floquet-East model corresponds to a Trotterisation of the standard continuous-time East model, which means that our results here provide an exact proof of dynamical hydrophobicity in that model, see [29]. These results highlight the usefulness of exact tensor network methods for studying many-body stochastic systems. One can think of many directions in which to expand the work here. These include studying circuit versions of other kinetically constrained models, generalisations to higher dimensions, and extensions to driven and non-equilibrium circuit systems.

Data availability statement

No new data were created or analysed in this study.

Acknowledgments

## Appendix. Finite space-time box in a large system

Since the time-evolution is bi-stochastic (see equation (14)) and the gate satisfies the kinetic constraint expressed by equation (15), a finite $l \times t$ space-time box embedded in a larger system (l.h.s. of figure 2) can be expressed as a finite system with special boundary conditions (r.h.s. of figure 2). To see this we consider the l.h.s. of figure 2, which we will refer to as $R_{l,t}$, and repeatedly apply the above relations everywhere in the system outside of the red box.

We start by applying the first of equation (14), which allows us to fully remove the top two rows of gates, and after touching the red box, we can continue applying the relation on the left and right removing everything except for the gates under the two diagonal lines as
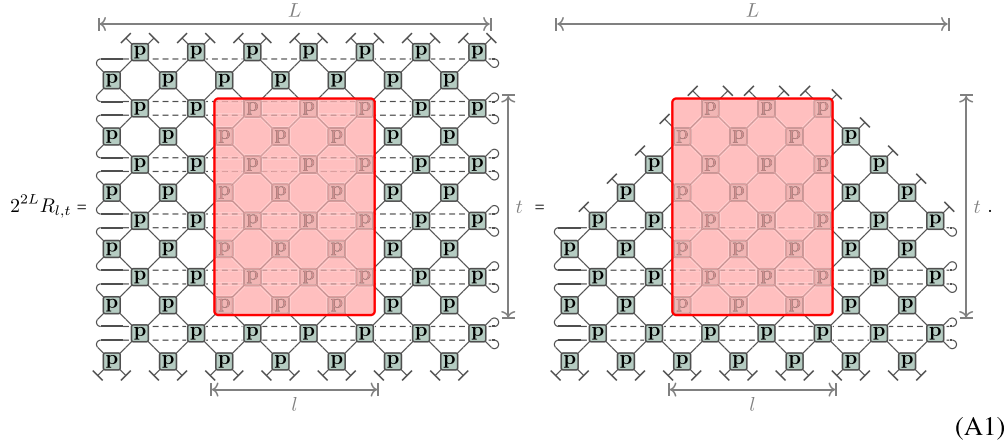
$$(A1)$$

Now we have no other gate where the first of equation (14) can be applied, but we are able to apply the second relation, which removes everything except for the rectangular box together with two triangular regions on the left and right,
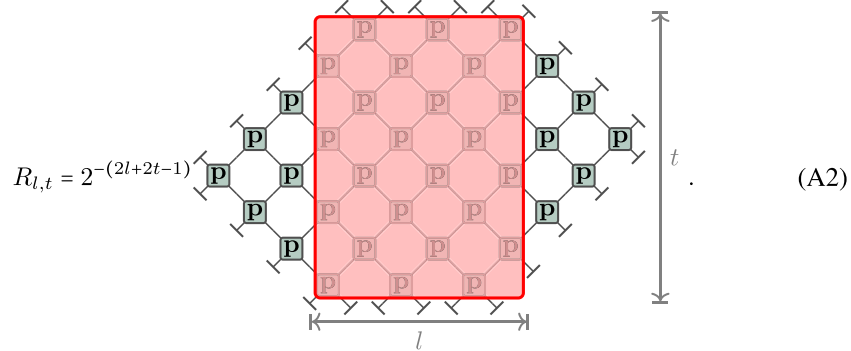
$$(A2)$$

Here we implicitly assumed that L is sufficiently large compared to l and t (in particular, $L \geqslant t + l - \frac{1}{2}$), which implies that there are no correlations between the left and right regions coming throughout the system. This is a strict form of the Lieb-Robinson bound [64], where the correlations outside of the light-cone are strictly zero (rather than exponentially suppressed). Note that to obtain the right prefactor we use the normalization of the $|-\rangle$ state, i.e. $\langle - \rangle = 2$.

The above form is very general and only depends on the bi-stochasticity of the time-evolution. However, the gates also fulfil the relations in (15), which additionally simplifies

the diagram. In particular, we note that applying two $|-\rangle$ states to the gate from the left simplifies it into the identity matrix on the right site,

$$\mathbf{P} = 2 \,(\, , \tag{A3}$$

which generalizes to the following for any number of vertically connected gates $m \geqslant 1$,

$$\tag{A4}$$

This immediately implies that the left triangle of gates in equation (A2) simplifies into a line, and we obtain

$$R_{l,t} = 2^{-(2l+t)} \Bigg(\qquad \Bigg)^{t}, \tag{A5}$$

which is precisely the r.h.s. of figure 2.

ORCID iDs

Cecilia De Fazio ⓘ https://orcid.org/0009-0007-1220-4771
Juan P Garrahan ⓘ https://orcid.org/0000-0002-0185-3924
Katja Klobas ⓘ https://orcid.org/0000-0001-6791-8594

References

[1] Ritort F and Sollich P 2003 *Adv. Phys.* **52** 219
[2] Garrahan J P, Sollich P and Toninelli C 2011 *Dynamical Heterogeneities in Glasses, Colloids and Granular Media* (*International Series of Monographs on Physics*), ed L Berthier G Biroli J-P Bouchaud L Cipelletti and W van Saarloos (Oxford University Press) ch 10, pp 341–66
[3] Berthier L and Biroli G 2011 *Rev. Mod. Phys.* **83** 587
[4] Biroli G and Garrahan J P 2013 *J. Chem. Phys.* **138** eid12A301
[5] Garrahan J P 2018 *Physica* A **504** 130

 [6] Chandler D and Garrahan J P 2010 *Annu. Rev. Phys. Chem.* **61** 191
 [7] Speck T 2019 *J. Stat. Mech.* 084015
 [8] Garrahan J P and Chandler D 2003 *Proc. Natl Acad. Sci.* **100** 9710
 [9] Keys A S, Hedges L O, Garrahan J P, Glotzer S C and Chandler D 2011 *Phys. Rev.* X **1** 021013
[10] Hasyim M R and Mandadapu K K 2023 arXiv:2310.06584
[11] Jäckle J and Eisinger S 1991 *Z. Phys.* B **84** 115
[12] Sollich P and Evans M R 1999 *Phys. Rev. Lett.* **83** 3238
[13] Elmatad Y S, Chandler D and Garrahan J P 2009 *J. Phys. Chem.* B **113** 5563
[14] Merolle M, Garrahan J P and Chandler D 2005 *Proc. Natl Acad. Sci. USA* **102** 10837
[15] Lecomte V, Appert-Rolland C and van Wijland F 2007 *J. Stat. Phys.* **127** 51
[16] Garrahan J P, Jack R L, Lecomte V, Pitard E, van Duijvendijk K and van Wijland F 2007 *Phys. Rev. Lett.* **98** 195702
[17] Touchette H 2009 *Phys. Rep.* **478** 1
[18] Jack R L 2020 *Eur. Phys. J.* B **93** 74
[19] Klobas K, De Fazio C and Garrahan J P 2024 *Phys. Rev.* E **110** 020103
[20] Lum K, Chandler D and Weeks J D 1999 *J. Phys. Chem.* B **103** 4570
[21] Chandler D 2005 *Nature* **437** 640
[22] Gopalakrishnan S and Zakirov B 2018 *Quantum Sci. Technol.* **3** 044004
[23] Berenstein D and Zhao J 2021 arXiv:2102.05745
[24] Bertini B, De Fazio C, Garrahan J P and Klobas K 2024 *Phys. Rev. Lett.* **132** 120402
[25] Bertini B, Kos P and Prosen T 2024 *Phys. Rev. Lett.* **132** 080401
[26] Garrahan J P, Jack R L, Lecomte V, Pitard E, van Duijvendijk K and van Wijland F 2009 *J. Phys.* A **42** 075007
[27] Bañuls M C and Garrahan J P 2019 *Phys. Rev. Lett.* **123** 200601
[28] Garrahan J P and Chandler D 2002 *Phys. Rev. Lett.* **89** 035704
[29] Katira S, Garrahan J P and Mandadapu K K 2018 *Phys. Rev. Lett.* **120** 260602
[30] Katira S, Mandadapu K K, Vaikuntanathan S, Smit B and Chandler D 2016 *eLife* **5** e13150
[31] Prosen T and Mejia-Monasterio C 2016 *J. Phys. A: Math. Theor.* **49** 185003
[32] Prosen T and Buča B 2017 *J. Phys. A: Math. Theor.* **50** 395002
[33] Gopalakrishnan S 2018 *Phys. Rev.* B **98** 060302(R)
[34] Buca B, Garrahan J P, Prosen T and Vanicat M 2019 *Phys. Rev.* E **100** 020103
[35] Klobas K, Medenjak M, Prosen T and Vanicat M 2019 *Commun. Math. Phys.* **371** 651
[36] Klobas K and Prosen T 2020 *SciPost Phys. Core* **2** 10
[37] Alba V, Dubail J and Medenjak M 2019 *Phys. Rev. Lett.* **122** 250603
[38] Klobas K, Vanicat M, Garrahan J P and Prosen T 2020 *J. Phys. A: Math. Theor.* **53** 335001
[39] Wilkinson J W P, Klobas K, Prosen T and Garrahan J P 2020 *Phys. Rev.* E **102** 062107
[40] Iadecola T and Vijay S 2020 *Phys. Rev.* B **102** 180302
[41] Gombor T and Pozsgay B 2021 *Phys. Rev.* E **104** 054123
[42] Wilkinson J W P, Prosen T and Garrahan J P 2022 *Phys. Rev.* E **105** 034124
[43] Bertini B, Kos P and Prosen T 2019 *Phys. Rev. Lett.* **123** 210601
[44] Kos P, Bertini B and Prosen T 2021 *Phys. Rev.* X **11** 011022
[45] Kos P and Styliaris G 2023 *Quantum* **7** 1020
[46] Bertini B, Kos P and Prosen T 2018 *Phys. Rev. Lett.* **121** 264101
[47] Bertini B, Kos P and Prosen T 2019 *Phys. Rev.* X **9** 021033
[48] Bertini B, Kos P and Prosen T 2020 *SciPost Phys.* **8** 067
[49] Bertini B, Kos P and Prosen T 2020 *SciPost Phys.* **8** 068
[50] Piroli L, Bertini B, Cirac J I and Prosen T 2020 *Phys. Rev.* B **101** 094304
[51] Claeys P W and Lamacraft A 2020 *Phys. Rev. Res.* **2** 033032
[52] Claeys P W and Lamacraft A 2021 *Phys. Rev. Lett.* **126** 100603
[53] Bertini B, Kos P and Prosen T 2021 *Commun. Math. Phys.* **387** 597
[54] Jonay C, Khemani V and Ippoliti M 2021 *Phys. Rev. Res.* **3** 043046
[55] Kasim Y and Prosen T 2022 *J. Phys. A: Math. Theor.* **56** 025003
[56] Suzuki R, Mitarai K and Fujii K 2022 *Quantum* **6** 631
[57] Foligno A and Bertini B 2023 *Phys. Rev.* B **107** 174311
[58] Foligno A, Zhou T and Bertini B 2023 *Phys. Rev.* X **13** 041008
[59] Rampp M A, Moessner R and Claeys P W 2023 *Phys. Rev. Lett.* **130** 130402
[60] Liu C and Ho W W 2023 arXiv:2312.12239
[61] Tensor network (available at: https://tensornetwork.org/)

[62] While the activity 'avalanches' can be seen as reminiscent of those in non-equilibrium setups such as self-organised criticality [65], for KCMs such as the East model they correspond to spontaneous (and non-critical) fluctuations that occur in the equilibrium dynamics.

[63] Yu X-H, Wang Z and Kos P 2024 *Quantum* **8** 1260

[64] Lieb E H and Robinson D W 1972 *Commun. Math. Phys.* **28** 251

[65] Marković D and Gros C 2014 *Phys. Rep.* **536** 41